

Generation of high-quality mega-electron volt proton beams with intense-laser-driven nanotube accelerator

M. Murakami and M. Tanaka

Citation: *Appl. Phys. Lett.* **102**, 163101 (2013); doi: 10.1063/1.4798594

View online: <http://dx.doi.org/10.1063/1.4798594>

View Table of Contents: <http://apl.aip.org/resource/1/APPLAB/v102/i16>

Published by the [American Institute of Physics](#).

Additional information on *Appl. Phys. Lett.*

Journal Homepage: <http://apl.aip.org/>

Journal Information: http://apl.aip.org/about/about_the_journal

Top downloads: http://apl.aip.org/features/most_downloaded

Information for Authors: <http://apl.aip.org/authors>

ADVERTISEMENT



Goodfellow
metals • ceramics • polymers • composites
70,000 products
450 different materials
small quantities fast

www.goodfellowusa.com

Generation of high-quality mega-electron volt proton beams with intense-laser-driven nanotube accelerator

M. Murakami^{1,a)} and M. Tanaka²

¹*Institute of Laser Engineering, Osaka University, Osaka 565-0871, Japan*

²*Department of Engineering, Chubu University, Aichi 487-8501, Japan*

(Received 14 December 2012; accepted 20 February 2013; published online 22 April 2013)

An ion acceleration scheme using carbon nanotubes (CNTs) is proposed, in which embedded fragments of low- Z materials are irradiated by an ultrashort intense laser to eject substantial numbers of electrons. Due to the resultant characteristic electrostatic field, the nanotube and embedded materials play the roles of the barrel and bullets of a gun, respectively, to produce highly collimated and quasimonoenergetic ion beams. Three-dimensional particle simulations, that take all the two-body Coulomb interactions into account, demonstrate generation of quasimonoenergetic MeV-order proton beams using nanometer-size CNT under a super-intense electrostatic field $\sim 10^{14}$ V m⁻¹. © 2013 American Institute of Physics. [<http://dx.doi.org/10.1063/1.4798594>]

Ion acceleration driven by ultraintense ultrashort laser pulses has been intensively studied in the past decade because a number of future applications are expected, including cancer therapy,¹ compact neutron sources,² and ion-driven fast ignition³ for medicine, industry, and fusion energy, respectively. For practical use of the accelerated ions, it is crucial to produce high-quality beams that are monoenergetic and collimated.^{4–6} So far, work on the generation of quasimonoenergetic ions has been mainly based on a planar geometry. Other schemes with different geometries have been proposed using, for example, double-layer targets⁷ or gas jet target.⁸ Ramakrishna *et al.*⁹ reported experimental evidence for quasimonoenergetic spectra of accelerated protons using water droplets. However, to produce high-quality ion beams is still in the process of research and development. An overall review on laser-driven ion acceleration can be found in Ref. 10.

Carbon nanotubes (CNTs)¹¹ have extraordinary properties with respect to their material and mechanical properties. Usually, CNTs are used as solid-state devices operating at relatively low temperatures,^{12,13} and there have been no CNT applications at temperatures higher than 10⁹ K and at time durations shorter than 10 fs. Here, we propose an ion acceleration scheme with the use of CNTs, working at such an extreme circumstance. In the present concept dubbed a nanotube accelerator, a CNT, with fragments of low- Z materials embedded in it, is irradiated by an ultrashort intense laser to generate quasimonoenergetic collimated ion beams. Figure 1 is a schematic of the nanotube accelerator, in which gold atoms are chemically adsorbed¹⁴ to the monolayer of carbon atoms composing the CNT. Inside the CNT, two smaller nanotubes are embedded. Typically, the nanotube accelerator is irradiated by a 10–20 fs pulse having a laser intensity of between 10¹⁷ and 10¹⁸ W cm⁻². This ultrashort pulse duration corresponds to the characteristic time of a Coulomb explosion,^{15–18} which is of the order of $2\pi/\omega_{pi}$ where ω_{pi} is the ion plasma frequency. Under such conditions, low- Z materials such as hydrogen and carbon are fully ionized, while materials such as gold are substantially ionized having

$Z = 15\text{--}25$ at laser intensities¹⁹ of 10¹⁸ W cm⁻². Significant numbers of electrons are then blown off by the intense laser field within a few laser cycles.

The coaxial nanotubes composed of ions and remaining electrons generate a characteristic Coulomb potential defined by $\phi(\mathbf{r}) = \sigma \int_V |\mathbf{r} - \mathbf{r}'|^{-1} d\mathbf{r}'$, where \mathbf{r} and \mathbf{r}' are position vectors corresponding to the points to be observed and integrated, respectively, σ is the electric charge density, and V denotes the whole volume containing electric charges. Here, the system is postulated to be cylindrically symmetric, i.e., $\phi = \phi(r, z)$, where r and z denote the coordinates along the radial and axial directions of the CNT, respectively. In particular, the Coulomb potential at an arbitrary point on z -axis ($-\infty < z < \infty$) is given in a simple analytic form

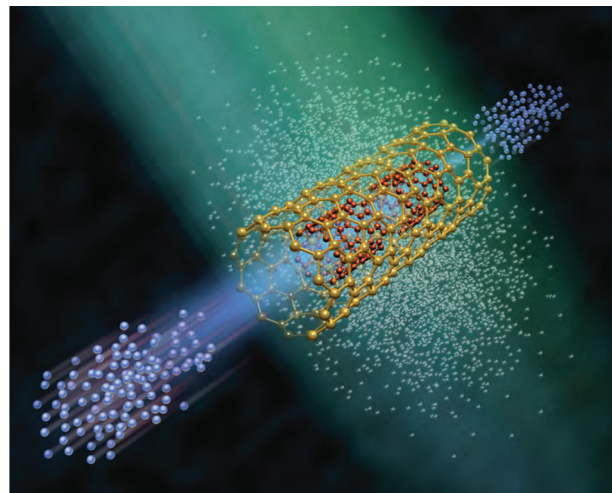


FIG. 1. Schematic view of a nanotube accelerator. The double nested nanotubes are irradiated by an ultrashort intense laser pulse. The outer carbon nanotube is chemically adsorbed with heavy atoms such as gold, while the inner nanotube is made of light materials such as hydrogen and carbon to form the bullets. Upon laser irradiation, electrons inside the nanotubes are ejected within a few laser cycles (comprising the small white particles around the nanotubes). The remaining nanotubes composed of positive ions generate a characteristic electrostatic Coulomb field so that the inner ions are accelerated along the axis symmetrically toward both ends of the outer nanotube. As a result, a pair of quasimonoenergetic collimated ion beams is obtained.

^{a)}Electronic address: murakami-m@ile.osaka-u.ac.jp

$$\phi(0, z) = 2\pi\sigma R \ln \left[\frac{\sqrt{R^2 + (z-L)^2} - (z-L)}{\sqrt{R^2 + (z+L)^2} - (z+L)} \right], \quad (1)$$

where the target center is set to be the origin of the coordinate system ($r = z = 0$), and $2R$ and $2L$ are the diameter and full axis-length of the cylindrical target. The potential given by Eq. (1) shows a one-humped structure with its peak at $z = 0$. In the limit of $z \rightarrow \infty$, Eq. (1) reduces to the well known form for a point charge, i.e., $\phi \rightarrow 4\pi\sigma RL|z|^{-1}$ as expected. Meanwhile, with respect to the behavior of ϕ along the r -axis, one can consider such a simplified physical picture without losing the essence that the axis length of the cylinder becomes null, i.e., $L \rightarrow 0$. Thus, we suppose such a circle of radius R , on which positive charges with a density per unit length, σ , are uniformly distributed. The resultant potential at a distance r from the center ($0 \leq r < \infty$) on the $z = 0$ plane is given by

$$\lim_{L \rightarrow 0} \phi(r, 0) = \frac{4\sigma R}{|R-r|} K \left[\frac{-4rR}{(R-r)^2} \right], \quad (2)$$

where the function K denotes the complete elliptic integral of the first kind. From Eq. (2), the potential turns out to monotonically increase such that $\phi = 2\pi\sigma \rightarrow \infty$ corresponding to $r = 0 \rightarrow R$ (the divergence to infinity at $r = R$ occurs only in the limit $L \rightarrow 0$). On the other hand, for the domain $R < r < \infty$, the potential ϕ monotonically decreases with r , and in the limit of $r \rightarrow \infty$, Eq. (2) asymptotically approaches $\phi \rightarrow 2\pi\sigma R r^{-1}$ again as in the point charge problem. Inside the nanotube, therefore, the electrostatic field has a saddle structure so that the potential surface is convex along z -axis and concave along r -axis.

Figure 2 shows a two-dimensional picture of the potential $\phi(r, z)$ obtained numerically, where $\sigma = 1$, $R = 1$, and $L = 2$ are employed just as an example. In Fig. 2, the influence of the inner low- Z nanotube upon ϕ is neglected because the total electric charge of the inner nanotube is much smaller than that of the outer nanotube. As a result of the saddle-shape potential, the interior ions get squeezed around the z -axis and accelerated along it, toward both ends of the CNT. Note that similar phenomenon to the squeezing effect has been reported, in which an injected diverging proton beam is bunched (squeezed) in a mm-long hollow cylindrical target.²⁰ Here we note, if electrons are distributed inside the cylinder, an electric field toward z -axis is generated, which is expected to enhance the squeezing effect. In Fig. 2, some test ions (red dots) are also depicted schematically how they are accelerated in the saddle-shaped potential field. The outer and inner nanotubes thus play the roles of the barrel and bullets of a gun, respectively. At positions around the CNT center, the potential gradients are relatively small along the z -axis. In other words, bullet ions initially located near the center will be accelerated quasimonoenergetically along the z -axis. It is also apparent from Eq. (1) that the outer nanotube should not be too long, or $L/R \sim \mathcal{O}(1)$, otherwise the field inside the CNT is mostly null, leading to a degraded performance as an accelerator. Meanwhile, heavy atoms such as gold, that are chemically adsorbed on the carbon atoms of the CNT,

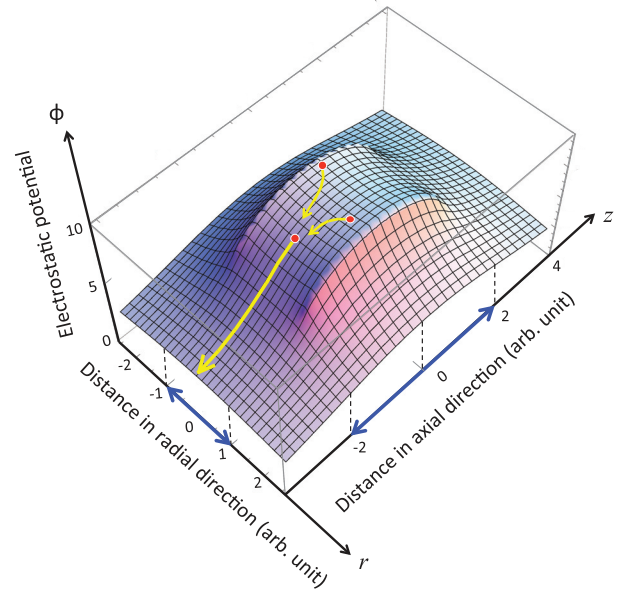


FIG. 2. Three-dimensional view of the Coulomb potential field projected onto the r - z plane. This potential is generated by the ionized outer nanotube, assuming the electric charge density is uniform over its cylindrical surface. The nanotube surface is defined by $-2 \leq z \leq 2$ along the cylindrical z -axis and by the cross section $x^2 + y^2 = 1$, corresponding to $|r| = 1$ on the r - z plane (highlighted by the blue arrows on the axes). The potential field inside the nanotube forms a saddle with a convex structure along the cylindrical z -axis and a weakly concave structure along the radial direction. Owing to this saddle shape, the bullet ions embedded in the nanotube are squeezed toward the central axis and slide down the potential surface to be ejected out of the nanotube with high collimation. Three test particles are schematically depicted how they move.

reinforce the gun barrel and considerably enhance the acceleration performance of the bullet ions.

We have performed N-body charged particle simulations, in which all of the particle-to-particle Coulomb forces are computed exactly. The relativistic version of the Newtonian equations of motion is used, similar to molecular dynamics simulations of microwave heating of salty water and ice.²¹ Moreover, our simulation includes the Lennard-Jones attractive potentials for pairs of like atoms and repulsive potentials for other species as a core exclusion to avoid numerical divergences. Such N-body simulations are the most suitable numerical approach for treating parametric domains in which the plasma scale becomes significantly shorter than the Debye length. Note that recombination is not included in the present numerical model, which is justified under such a circumstance seen in the present scheme that stripped electrons are distantly blown off. Figure 3 shows the temporal evolution of the dynamics of the nanotube accelerator, obtained from the N-body simulations. The CNT has an axial length of 30 nm and a diameter of 15 nm at which the gold atoms are chemically adsorbed to the carbon atoms. Inside the CNT, two cylindrical bullet nanotubes made of hydrogen are embedded, each of which has a diameter of 6 nm and an axial length of 6 nm. The initial distance between the two hydrogen bullets is 8 nm. Although hydrogen nanotubes do not actually exist in nature, it does not alter the physical mechanism of the nanotube accelerator, because the ionized bullets lose their original shape as they are squeezed toward the axis (see the time sequence of the top views in Fig. 3). Although it is not our main issue to elaborate the

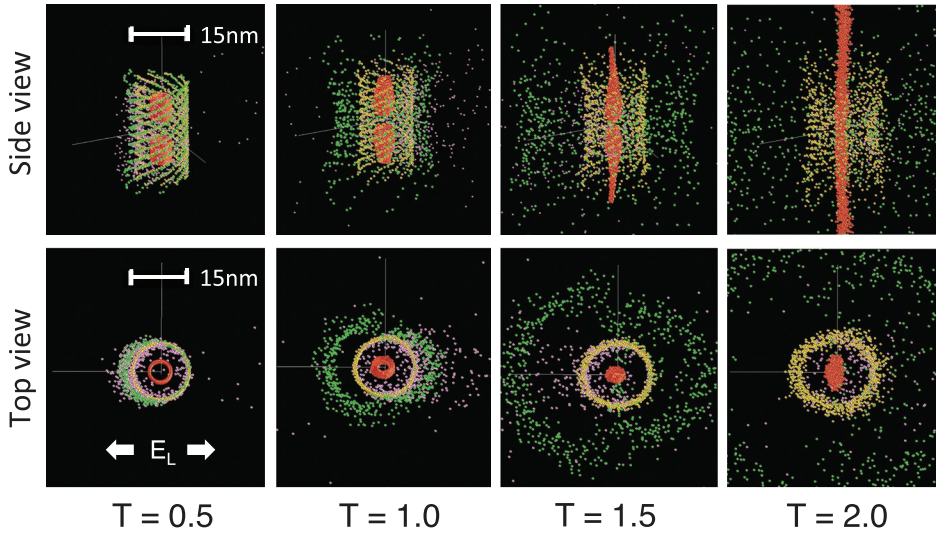


FIG. 3. Snapshots of the nanotube accelerator dynamics at sequential times, obtained by the N-body simulations in a side view (upper row) and top view (lower row). The outer nanotube is of 30 nm in length and 15 nm in diameter, with gold atoms (yellow) chemically adsorbed onto the carbon atoms (green). Inside the nanotube, two cylindrical bullet nanotubes made of hydrogen (red) are embedded. Sinusoidal laser light is applied with intensity $I_L = 10^{18} \text{ W cm}^{-2}$. During the first laser cycle, ionized electrons (white) are ejected by the laser field. Simultaneously, the saddle-shaped Coulomb field in Fig. 2 forms to squeeze and accelerate the bullet ions along the z-axis.

practical target fabrication, we here give a few descriptions from an engineering point of view: The use of pure hydrogen clusters as the bullets is unpractical, because solid hydrogen atoms exist only at extremely low temperatures at around -250°C . However, they can be easily replaced by such a hydrogen compound as water (H_2O) or paraffin (C_nH_{2n}) that can be solid at room temperatures ($\geq 0^\circ\text{C}$). When such a compound is decomposed into fully ionized ions when irradiated by an intense laser, protons are to be selectively accelerated at higher quasimonoenergetic speeds.¹⁸ Pure carbon compounds like fullerenes or CNT are also tractable materials for the bullet. Insertion of nanometer-size structures into CNTs is another key issue. For example, producing CNTs containing fullerenes inside²² or multi-walled carbon nanotubes (MWCNT)²³ has already been well established technically. Note that the size of the nanotube accelerator in Fig. 3 is the largest one that can be treated in our numerical environment using real lattice constants for the materials. The total number of charged particles for our simulations is about 4×10^5 .

At $t = 0$, sinusoidal laser light is incident on the nanotube from a radial direction perpendicular to the axis. The linearly polarized electric field is $E_L = E_0 \sin(2\pi T)$ for $T > 0$, where $T = t/t_0$ is the time normalized to the laser period $t_0 = 2.7 \text{ fs}$ for a titanium-sapphire laser at a wavelength of $\lambda_L = 0.8 \mu\text{m}$. In Fig. 3, the field amplitude is $E_0 = 3 \times 10^{12} \text{ V m}^{-1}$, corresponding to a laser intensity of $I_L = 10^{18} \text{ W cm}^{-2}$. At such an intensity, the gold atoms are photoionized to a state of about $Z_{\text{Au}} = 20$,¹⁴ while the carbon and hydrogen atoms are fully ionized to $Z_{\text{C}} = 6$ and $Z_{\text{H}} = 1$, respectively. Note that, in the present simulation, the averaged number of electrons that are effectively blown off from the nanotube is observed to be $Z_{\text{eff}} = 17 - 18$ per single gold ion. The maximum ion kinetic energy is expected to increase with the system size and laser intensity according to the principles of a Coulomb explosion.¹⁸

In Fig. 3, the four snapshots correspond to the duration of the first two laser cycles ($T \leq 2$) at a constant increment of $\Delta T = 0.5$. During the first cycle, many electrons are ejected by the intense laser field, which are already driven far away at the snapshot times and cannot be seen in Fig. 3. Simultaneously, the saddle-shaped Coulomb field of Fig. 2

forms to squeeze and accelerate the bullet ions along the z-axis. Quantitative performance is plotted in Fig. 4, where the spectrum of the kinetic energy component along the z-direction, E_z , is seen to form a sharp quasimonoenergetic profile at normalized times of between $T = 4$ and 5. With the parameters that can be managed in our numerical environment, the energy is limited to $\mathcal{E}_{\text{max}} = 1.5 \text{ MeV}$. The acceleration distance is roughly the half of the outer nanotube $\sim 15 \text{ nm}$, that corresponds to an electrostatic force of the order of 10^{14} V m^{-1} , which is much higher than, for instance, a typical value expected in laser-plasma wakefield acceleration.²⁴ As long as monolayered nanotubes (in two dimensions) are used, the achievable ion energy \mathcal{E}_{max} is expected to increase linearly with the nanotube size L . If the nanotubes have a finite thickness (i.e., are three-dimensional), then one obtains another scaling law, $\mathcal{E}_{\text{max}} \propto L^2$. Furthermore, if the hydrogen atoms are replaced by carbon atoms, the kinetic energy of

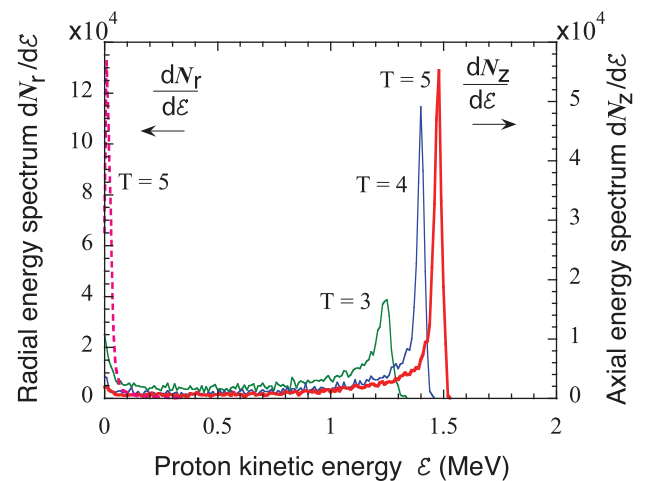


FIG. 4. Temporal evolution of the proton energy spectrum in the axial (solid curves) and radial (dashed curve at $T = 5$) directions. The corresponding two-dimensional dynamics are shown in Fig. 3. Quasimonoenergetic protons with an energy of $\mathcal{E}_{\text{max}} = 1.5 \text{ MeV}$ are produced at $T = 5$. If the hydrogen atoms are replaced by carbon atoms, the maximum ion energy increases to about 10 MeV for the same target structure. The maximum energy can also be increased by enlarging the target size. The energy ratio $\bar{\mathcal{E}}_z/\bar{\mathcal{E}}_r \approx 85$ at $T = 5$ indicates high collimation in the present scheme, where $\bar{\mathcal{E}}_z$ and $\bar{\mathcal{E}}_r$ are the average proton kinetic energies in the axial and radial directions, respectively.

each carbon ion increases to about 10 MeV (the kinetic energy per nuclei is a bit smaller than in the proton case) for the same target structure as in Fig. 3, because the kinetic energy results from the initial potential energy which in turn is proportional to the electric charge. Note that for more practical simulations, one needs to take account of a realistic laser pulse shape with a smooth envelope. As a matter of fact, we have verified that a quantitatively similar result to Fig. 3 in view of the energy spectrum is obtained using a Gaussian pulse with a full width at half maximum (FWHM) of five laser cycles under the same peak intensity. Retardation and magnetic effects in the electron-electron interactions will become crucial in the highly relativistic regime. However, working laser intensities for the present size of the CNT are expected to be $I_L \lesssim 10^{18} \text{ W cm}^{-2}$, and the relativistic effects mentioned above are not crucial.

A good measure of the collimation is $\bar{\mathcal{E}}_z/\bar{\mathcal{E}}_r$, where $\bar{\mathcal{E}}_z$ and $\bar{\mathcal{E}}_r$ denote the average kinetic energies of the bullet ions in the axial and radial directions, respectively. As was seen in Fig. 3, the bullet ions are accelerated with a good collimation along z -axis. This longitudinal kinetic energy is approximately equal to the initial Coulomb energy, i.e., $\bar{\mathcal{E}}_z \approx q(Q/X)_{\text{out}}$, where Q and X are the total electric charge and a characteristic length of the outer nanotube in the early stage of the Coulomb explosion, respectively; q is the electric charge of the bullet ion. The scale length X can be approximately given by $X \approx \min(R, L)$. Here, it should be noted that the present preliminary numerical survey has revealed that the aspect ratio of the outer nanotube in the range, $2 \lesssim L/R \lesssim 3$, seems to be crucial to produce high-quality ion beams. Meanwhile, the lateral (radial) kinetic energy of the bullet ions is brought about mainly by their own Coulomb repulsion, i.e., $\bar{\mathcal{E}}_r \approx q(Q/X)_{\text{in}}$, where $(Q/X)_{\text{in}}$ is defined quite in a similar manner to $(Q/X)_{\text{out}}$ but for the inner nanotube. Thus, the energy ratio is estimated by

$$\frac{\bar{\mathcal{E}}_z}{\bar{\mathcal{E}}_r} \approx \frac{(Q/X)_{\text{out}}}{(Q/X)_{\text{in}}}. \quad (3)$$

In the case of Fig. 4, $\bar{\mathcal{E}}_z \approx 1.5 \text{ MeV}$ and $\bar{\mathcal{E}}_r \approx 0.017 \text{ MeV}$ in the final stage of acceleration, so that $\bar{\mathcal{E}}_z/\bar{\mathcal{E}}_r \approx 85$, which is rather close to a rough estimate obtained from Eq. (3), $\bar{\mathcal{E}}_z/\bar{\mathcal{E}}_r \sim 100$. These values of $\bar{\mathcal{E}}_z/\bar{\mathcal{E}}_r$ indicate a remarkably high degree of collimation in spite of the relatively small aspect ratio of the CNT structure, i.e., $L/R = 2$. If the accelerated protons are kept ionized in flight without recombination, they are subject to long-range Coulomb forces. It might then be conjectured that the collimation performance of the beams can be degraded even at later times. However, the size of the bullet materials at $T \gtrsim 5 - 10$ is already much larger than the initial size. In this stage, most of the Coulomb energy has already been converted into the kinetic energy, and thus the collimation will not be substantially degraded at later times.

Finally, the energy coupling efficiency η_c is an important index of the ion beam generation from an engineering point of view. It is defined as the ratio of the integrated kinetic energy of the bullet ions to that of all the electrons and ions at $t \rightarrow \infty$. The latter balances with the absorbed laser energy. In practical cases, the absorption efficiency of the system depends on how many nanotubes are set in the focal

region as well as the microscopic nanotube structure. In the present work, where the system is not optimized yet, the values of η_c are of the order of 1% or less.

In summary, we have proposed an ion acceleration scheme using structured nanotubes that operate under irradiance of ultrashort ultraintense laser pulses, to produce high-quality ion beams. Detailed three-dimensional particle simulation has demonstrated the generation of quasimonoenergetic highly collimated 1.5-MeV proton beams. It has been demonstrated that spacial control in nano-scale fabrication is as effective as temporal control in femto-scale laser operation. For further practical studies of the present scheme, it will be crucial that multiple nanotubes are uniformly produced in size and uniformly arranged in direction.

This work was supported by Japan Society for the Promotion of Science (JSPS). One of the authors (M.T.) thanks Dr. M. Yamashiro for discussions about carbon nanotubes. Present simulations were performed using Hitachi SR16000 system of National Institute for Fusion Science, Japan.

- ¹S. S. Bulanov, A. Brantov, V. Yu. Bychenkov, V. Chvykov, G. Kalinchenko, T. Matsuoka, P. Rousseau, S. Reed, V. Yanovsky, D. W. Litzenberg, and A. Maksimchuk, *Med. Phys.* **35**, 1770 (2008).
- ²T. Ditmire, J. Zweiback, V. P. Yanovsky, T. E. Cowan, G. Hays, and K. B. Wharton, *Nature* **398**, 489 (1999).
- ³M. Roth, T. E. Cowan, M. H. Key, S. P. Hatchett, C. Brown, W. Fountain, J. Johnson, D. M. Pennington, R. A. Snavely, S. C. Wilks, K. Yasuike, H. Ruhl, F. Pegoraro, S. V. Bulanov, E. M. Campbell, M. D. Perry, and H. Powell, *Phys. Rev. Lett.* **86**, 436 (2001).
- ⁴S. C. Wilks, A. B. Langdon, T. E. Cowan, M. Roth, S. Singh, S. Hatchett, M. H. Key, D. Pennington, A. MacKinnon, and R. A. Snavely, *Phys. Plasmas* **8**, 542 (2001).
- ⁵T. E. Cowan, J. Fuchs, H. Ruhl, A. Kemp, P. Audebert, M. Roth, R. Stephens, I. Barton, A. Blazevic, E. Brambrink, J. Cobble, J. Fernandez, J. C. Gauthier, M. Geissel, M. Hegelich, J. Kaae, S. Karsch, G. P. Le Sage, S. Letzring, M. Manclossi, S. Meyroneinc, A. Newkirk, H. Pepin, and N. Renard-LeGalloudec, *Phys. Rev. Lett.* **92**, 204801 (2004).
- ⁶B. M. Hegelich, B. J. Albright, J. Cobble, K. Flippo, S. Letzring, M. Paffett, H. Ruhl, J. Schreiber, R. K. Schulze, and J. C. Fernández, *Nature* **439**, 441 (2006).
- ⁷T. Esirkepov, M. Borghesi, S. V. Bulanov, G. Mourou, and T. Tajima, *Phys. Rev. Lett.* **92**, 175003 (2004).
- ⁸K. Krushelnick, E. L. Clark, Z. Najmudin, M. Salvati, M. I. K. Santala, M. Tatarakis, A. E. Dangor, V. Malka, D. Neely, R. Allott, and C. Danson, *Phys. Rev. Lett.* **83**, 737 (1999).
- ⁹B. Ramakrishna, M. Murakami, M. Borghesi, L. Ehrentraut, P. V. Nickles, M. Schnürer, S. Steinke, J. Psikal, V. Tikhonchuk, and S. Ter-Avetisyan, *Phys. Plasmas* **17**, 083113 (2010).
- ¹⁰H. Daido, M. Nishiuchi, and A. S. Pirozhkov, *Rep. Prog. Phys.* **75**, 056401 (2012).
- ¹¹S. Iijima, *Nature* **354**, 56 (1991).
- ¹²B. Gao, C. Bower, J. D. Lorentzen, L. Fleming, and A. Kleinhammes, X. P. Tang, L. E. McNeil, Y. Wu, and O. Zhou, *Chem. Phys. Lett.* **327**, 69 (2000).
- ¹³D. A. Walters, M. J. Casavant, H. C. Qin, C. B. Huffman, P. J. Boul, L. M. Ericson, E. H. Haroz, M. J. O'Connell, M. J. K. Smith, D. T. Colbert, and R. E. Smalley, *Chem. Phys. Lett.* **338**, 14 (2001).
- ¹⁴Y. T. Kim, K. Ohshima, K. Higashimine, T. Uruga, M. Takata, H. Suematsu, and T. Mitani, *Angew. Chem., Int. Ed.* **45**, 407 (2006).
- ¹⁵K. Nishihara, H. Amitani, M. Murakami, S. V. Bulanov, and T. Zh. Esirkepov, *Nucl. Instrum. Methods Phys. Res. A* **464**, 98 (2001).
- ¹⁶V. N. Novikov, A. V. Brantov, V. Yu. Bychenkov, and V. F. Kovalev, *Plasma Phys. Rep.* **34**, 920 (2008).
- ¹⁷Y. Fukuda, A. Ya. Faenov, M. Tampo, T. A. Pikuz, T. Nakamura, M. Kando, Y. Hayashi, A. Yogo, A. H. Sakaki, T. Kameshima, A. S. Pirozhkov, K. Ogura, M. Mori, T. Zh. Esirkepov, J. Koga, A. S. Boldarev, V. A. Gasilov, A. I. Magunov, T. Yamauchi, R. Kodama, P. R. Bolton, Y. Kato, T. Tajima, H. Daido, and S. V. Bulanov, *Phys. Rev. Lett.* **103**, 165002 (2009).

- ¹⁸M. Murakami and K. Mima, [Phys. Plasmas](#) **16**, 103108 (2009).
- ¹⁹P. Mulser and D. Bauer, *High Power Laser-Matter Interaction* (Springer, Berlin, Heidelberg, 2010), Chap. 7.
- ²⁰T. Toncian, M. Borghesi, J. Fuchs, E. d'Humieres, P. Antici, P. Audebert, E. Brambrink, C. A. Cecchetti, A. Pipahl, L. Romagnani, and O. Willi, [Science](#) **312**, 410 (2006).
- ²¹M. Tanaka and S. Sato, [J. Chem. Phys.](#) **126**, 034509 (2007).
- ²²B. W. Smith, M. Monthieux, and D. E. Luzzi, [Nature](#) **396**, 323 (1998).
- ²³X. Zhao, M. Ohkohchi, M. Wang, S. Iijima, T. Ichihashi, and Y. Ando, [Carbon](#) **35**, 775 (1997).
- ²⁴T. Tajima and J. M. Dawson, [Phys. Rev. Lett.](#) **43**, 267 (1979).